



## Improving Mobile Platform Gaussian-Derived Emission Estimates Using Hierarchical Sampling and Large Eddy Simulation

Dana R. Caulton<sup>1</sup>, Qi Li<sup>2</sup>, Elie Bou-Zeid<sup>1</sup>, Jessica Lu<sup>1</sup>, Haley M. Lane<sup>1</sup>, Jeffrey P. Fitts<sup>1</sup>, Bernhard Buchholz<sup>3</sup>, Levi M. Golston<sup>1</sup>, Xuehui Guo<sup>1</sup>, James McSpirtt<sup>1</sup>, Da Pan<sup>1</sup>, Lars Wendt<sup>4</sup> and Mark A. Zondlo<sup>1</sup>

<sup>1</sup>Department of Civil and Environmental Engineering, Princeton University, 59 Olden St., Princeton, NJ 08540, U.S.A.

<sup>2</sup>Department of Earth and Environmental Engineering, Columbia University, 500 W 120<sup>th</sup> St., New York, NY 10027, U.S.A.

<sup>3</sup>RMS, Technische Universität Darmstadt, Darmstadt, 64287, Germany

<sup>4</sup>Hunterdon Central Regional High School, Flemington, NJ 08822, U.S.A.

Correspondence to: M. A. Zondlo ([mzondlo@princeton.edu](mailto:mzondlo@princeton.edu))

**Abstract.** Mobile laboratory measurements provide information on the distribution of CH<sub>4</sub> emissions from point sources such as oil and gas wells, but uncertainties are poorly constrained or justified. Sources of uncertainty and bias in ground-based Gaussian derived emissions estimates from a mobile platform were analyzed in a combined field and modeling study. In a field campaign where 1009 natural gas sites in Pennsylvania were sampled, a hierarchical measurement strategy was implemented with increasing complexity. Of these sites, ~93% were sampled with an average of 2 transects (standard sampling), ~5% were sampled with an average of 10 transects (replicate sampling) and ~2% were sampled with an average of 20 transects while simultaneously deploying a tower to measure high-frequency meteorological data (intensive sampling). Five of the intensive sampling sites were modeled using large eddy simulation (LES) to reproduce CH<sub>4</sub> concentrations in a turbulent environment. The LES output and derived emission estimates were used to compare with the results of a standard Gaussian approach. The LES and Gaussian derived emission rates agreed within a factor of 2, in most cases with average differences of 25%. A controlled release was also used to investigate sources of bias in either technique. The Gaussian agreed with the release rate more closely than the LES underlying the importance of inputs as sources of uncertainty for the LES. The LES was also used as a virtual experiment to investigate optimum number of repeat transects and spacing needed to produce representative statistics. Approximately 10 repeat transects spaced at least 1 min apart are required to produce statistics similar to the observed variability over the entire LES simulation period of 30 min. In addition, other sources of uncertainty including source location, wind speed and stability were analyzed. In total, atmospheric variability, observed by repeat measurements at individual sites under relatively constant conditions, was found to be the most significant contributor to total uncertainty. Accurate measurements of this condition provide a reasonable estimate of the lower bound for emission uncertainty. It is recommended that future mobile monitoring schemes quantify this metric under representative conditions to accurately estimate emission uncertainty.



## 1 Introduction

Reducing emissions of short-lived greenhouse gases through regulations has been considered a potentially viable way to mitigate climate change without intensively regulating CO<sub>2</sub>, which poses economic and political challenges. In particular, reducing CH<sub>4</sub>, a potent greenhouse gas and the main component of natural gas, may have significant immediate climate benefits (Bowerman et al., 2013, Baker et al., 2015, Zickfeld et al., 2017) and be a viable mitigation option. However, the large numbers and types of components in the natural gas supply chain that may leak require the development of efficient and accurate methods to quantify emissions. Specifically, techniques are needed that are available to researchers at every level (government, industry and academic), accurate enough to locate and quantify specific sources of fugitive emissions and allow for self-monitoring, independent verification and understanding of common leak sources.

To this end, various independent CH<sub>4</sub> emission estimation techniques have been implemented. Table 1 shows the methods that have been primarily applied to oil, coal and gas extraction and infrastructure which account for ~30% of the total global anthropogenic CH<sub>4</sub> emissions (Kirschke et al., 2013). The myriad of sites and types of emission sources have necessitated the development and application of multiple techniques. Examples include satellites (Kort et al., 2014) remote sensing from aircraft (Kuai et al., 2016, Frankenberg et al., 2016, Thorpe et al., 2016), in-situ aircraft measurements (Karion et al., 2013 and 2014, Peischl et al., 2013 and 2015, Caulton et al., 2014, Petron et al., 2014, Lavoie et al., 2015, Ren et al., 2017), long-term monitoring from short and tall towers (Petron et al., 2012), unmanned aerial vehicles (Nathan et al., 2015) and various ground-based techniques. Ground-based techniques include flask sampling (Townsend-Small et al., 2015), tracer correlation techniques (Lamb et al., 2015, Subramanian et al., 2015, Zimmerle et al., 2015, Omara et al., 2016), chamber sampling (Allen et al., 2013 and 2014, Kang et al., 2014), thermal/optical imaging (Galfalk et al., 2015, Ravikumar et al., 2017) and combined measurement/dispersion modeling techniques from stationary (Brantley et al., 2014, Foster-Witting et al., 2015) and mobile platforms (Lan et al., 2015, Rella et al., 2015, Yacovitch et al., 2015).

Every technique has considerable advantages and disadvantages related to operational cost, sampling efficiency, processing time and uncertainty. Table 1 compares the author reported uncertainties for several techniques. These uncertainty estimates should be compared with caution: self-reported uncertainties are not computed in identical manners and some may not include the same sources of uncertainty in their considerations or additional systematic biases to the same extent. The values reported for *emission* uncertainties, usually significant, are generally not from *measurement* uncertainties. Even instruments that produce high accuracy measurements that must be transformed into an emission rate can be confounded by transformation methods that rely upon limited or unrepresentative meteorological conditions such as small scale turbulence characterization, boundary layer processes or assigning background conditions to a variable atmosphere. Notable, however, is the large range of uncertainties reported by ground-based mobile dispersion techniques. These techniques rely on accurate and precise concentration measurements coupled with dispersion models (Gaussian, AERMOD, WindTrax, etc.) to produce an emission estimate and are subject to various uncertainties in the model, notably atmospheric diffusion coefficients. These techniques are attractive due to their relatively low cost, computational requirements and high sampling efficiency of individual



sources. However, as seen in Table 1, current results lag behind the standard for other measurement techniques in this field. Therefore there is a critical need for improved sampling methods and/or data processing in this field to close the gap between data quality.

### 1.1 Theory of the Gaussian Plume Model

5            Approximations of scalar dispersion were investigated as early as the 1930s and were developed to describe non-reactive pollutant dispersal from elevated stacks (Sutton, 1932; Bosanquet and Pearson, 1936). As models improved, the Gaussian plume model was developed assuming that scalar concentration has a normal distribution function (Batchelor, 1949, Hilst, 1957). Additional investigation of near surface conditions where particles can either deposit to or reflect off the surface led to the current Gaussian plume analytical model (shown in Eq. 1), which can be directly derived from the advection–  
10    diffusion equation under some simplifying assumptions (as explained in Veigele and Head, 1978). Variations of this equation can be found in many papers and textbooks (for example Gifford, 1968, Zannetti, 1990).

$$C(x, y, z) = \frac{Q}{2\pi\sigma_y\sigma_z u} \cdot e^{-\frac{y^2}{2\sigma_y^2}} \cdot \left[ e^{-\frac{(z-h)^2}{2\sigma_z^2}} + e^{-\frac{(z+h)^2}{2\sigma_z^2}} \right] \quad (1)$$

This function relies on the 3-D distances  $(x, y, z)$  of a receptor from a source as well as the source height  $h$ , mean horizontal wind speed  $u$ , and a source strength,  $Q$ . The dispersion coefficients  $(\sigma_y, \sigma_z)$  encode the strength of turbulent mixing and are  
15    calculated according to any of several analytical parameterizations based on Pasquill-Gifford's stability class scheme. Atmospheric stability classes range from very unstable (A) to very stable (F). Class D is defined as neutral. The model describes the probability density function (pdf) of a scalar concentration ( $C$ ) downwind of a source, meaning it describes average plume locations and concentrations. However, the instantaneous observed plume structure deviates greatly from the average behavior, with fluctuating peak concentration location and displaying lower or higher concentration.

20            The Gaussian plume model is used to calculate emissions by comparing the model output to the observations. This can be done in a variety of ways. The stationary dispersion techniques used by Brantley et al. (2014) and Foster-Wittig et al. (2015) utilize the model at a single point and relate changes in concentration to changes in wind direction and thus speed. These procedures either follow or are related to the well-defined U.S. EPA OTM 33a and are not discussed further. The mobile dispersion techniques investigated in this study and others (Lan et al., 2015, Rella et al., 2015, Yacovitch et al., 2015) compare  
25    observed concentrations at continuous downwind  $x$  and  $y$  locations (i.e. along a road) to the modeled output along this road. Various techniques have also incorporated averaging schemes and additional  $z$  dimensional data (Lan et al., 2015, Rella et al., 2015). Wind direction and speed are either fixed to the prevailing direction or rotated to match the observations. While data can be collected and processed quickly, the application of a Gaussian model that describes average plume behavior to instantaneous data has apparent shortcomings and no standard uncertainty protocol has been established.



## 1.2 Previous Work

Robust uncertainty analyses of Gaussian emission retrievals are not reported in most studies, which instead focus on the novel application of the methods. Yacovitch et al. (2015) reported an asymmetric 95% confidence interval on their emission rates of  $0.334(x) - 3.34(x)$  where  $x$  is the reported emission rate by using a controlled release as a proxy. Lan et al. (2015) used a Monte Carlo approach based on assumed uncertainty in source height, wind speed and wind direction for an average 95% confidence interval of roughly  $0.5(x) - 1.5(x)$ . Rella et al. (2015) also used a controlled release to calculate the variation in their measurement of a constant emission and reported a 95% confidence interval of  $0.28(x) - 3.6(x)$ . These methods report uncertainty methods that are comparable in nature. Notably, Lan et al.'s (2015) Monte Carlo method produced the smallest confidence interval, but accounted only for assumed uncertainty in three parameters and may neglect other factors (distance, stability, emission variability). The controlled release method employed by Yacovitch et al. (2015) and Rella et al. (2015) is useful in that direct observations of measurement variability can be made and potential bias in the measurements can be determined. However, these methods produce large uncertainty ranges that may be unsuitable to reliably separate large emissions from normal emissions. Additionally, implementing a controlled release is not trivial due to long set-up times of equipment and restricted access to locations suitable for the release. These conditions may make a controlled release experiment prohibitive for many applications with strict time or budget constraints or for those where site access is limited.

The Gaussian model is attractive as a method for inferring emission rates as it is fast and generalizable with the ability to account for changes in stability, wind speed and source elevation. However, the uncertainties for this method change depending upon how it is implemented and whether it is extended to situations outside the reasonable limits of the generalized form. Such situations would include using an average plume for unconstrained instantaneous measurements or modeling over complex topography. A method for implementation of this technique is needed that identifies best practices and is supported by observations and modeling.

In our study, we combine traditional Gaussian methods, advanced large eddy simulation modeling and a controlled release to assess in situ variability of emission retrievals from  $\text{CH}_4$  plumes downwind of natural gas well pads in the Marcellus Shale in Pennsylvania. We also investigate sources of potential bias in the controlled release and modeling methods. The basic architecture of this method uses (1) advanced modeling of a preselected sample site to enable investigation of optimum sampling strategies, (2) application of strategies to our sample collection process and (3) evaluation of additional sources of uncertainty and bias using advanced modeling and a controlled release.

## 2 Methods

### 2.1 Instrumentation

Data were collected in Pennsylvania during three campaigns in July 2015, November 2015 and June 2016 using the Princeton Atmospheric Chemistry Experiment (PACE). A Honda CR-V has been modified to accommodate a roof rack that



hold sensors ~1 m above the car, to limit the possibility of self-sampling. The roof rack is equipped with a LICOR 7700 to measure CH<sub>4</sub> and LICOR 7500A to measure CO<sub>2</sub> and H<sub>2</sub>O; both sensors record at 10 Hz. Meteorological data and GPS data were collected at 1 Hz with a Vaisala WXT520 and Garmin unit in July 2015 and June 2016 and with an Airmar WS-200WX in November 2015. More information on the mobile lab design and instrumentation can be found in Tao et al. 2015. The  
5 LICOR sensors were calibrated prior to each campaign using a blank (N<sub>2</sub>) and a 2.12 ppm CH<sub>4</sub> standard in air and were also periodically calibrated with a  $1.8724 \pm 0.0030$  ppm CH<sub>4</sub> and  $394.51 \pm 0.07$  ppm CO<sub>2</sub> NOAA standard. Data were synchronized and logged using a custom LabVIEW program.

In addition, at select sites a tower was set up to measure high-frequency meteorological data. This tower included a second pair of LICOR 7500A and 7700 along with a METEK uSonic-3 Class A sonic anemometer to measure 3-D wind  
10 components. The tower was typically set alongside the road at a height between 2 and 3 m. Initially, the tower was constructed using a standard tripod, but was later adapted to the bed of a pick-up truck to allow faster deployment. The air flow around the pick-up truck was modeled (using Fluent, <http://www.ansys.com/Products/Fluids/ANSYS-Fluent>) to determine optimum placement of sensors above the vehicle to minimize local flow distortions. Three orientations were tested, with the truck cab facing 0°, 90° and 180° with a 0° mean wind flow. Deflection was observed in all three cases, but the distortion was minimal  
15 at ~2 m above the pickup bed. The final design of the mobile lab, the instrumentation rack and the mobile tower is shown in Fig. 1.

## 2.2 Site Sampling

Unconventional natural gas well pads were selected before sampling using a pseudo-random method. All datasets were accessed from the Pennsylvania Spatial Data ACCESS ([www.pasda.psu.edu](http://www.pasda.psu.edu)). Sites were screened for distance (<300 m  
20 from public road), obstructions (elevation difference >50 m, trees) and wind direction. These characteristics were determined to be the most crucial for successfully sampling sites in this area as topography and vegetation made detecting plumes farther than 300 m difficult as the source could not be visually verified. Routes were primarily planned for efficiency around the forecast mean wind direction; however, the distribution of the sample relative to the population of key factors (well age, production, and operator) was routinely examined to identify and correct for over- and under- representation. Additional details  
25 on the sampling strategy can be found in Sect. 3.

As a source of validation, an experimental controlled release of CH<sub>4</sub> was also performed. The controlled release allows the retrieved emissions to be compared to known emission rates from a constant source. A pure (99.5%) CH<sub>4</sub> cylinder was vented at various controlled flow rates to produce different measurable emission rates. The release site was selected for flat, open topography and isolated from any potential sources. Background transects were collected for approximately 30 min  
30 before the experiment to ensure no contaminating signals would be detected. An interfering signal from a large mulch pit was detected and the release set up was moved away from the source to ensure no signal mixing. The cylinder was set ~100 m from a public road at an altitude of 1 m. The release was performed over several hours, during afternoon and evening to span different stability classes. Figure S1 shows a diagram of the release set-up.



### 2.3 Inverse Gaussian Method (IGM)

The IGM approach has been used extensively as described in Sect. 1.1. Applied here, the method uses the sampled source location as input to first identify downwind transects. Transect selection must be finalized by the user. The peak CH<sub>4</sub> location is assumed to correspond to the prevailing wind direction and centerline plume direction ( $x$  in Eq. 1). The along-wind and across-wind ( $y$  in Eq. 1) distances are then calculated using the synchronous GPS data. Distances are calculated for each measurement point as a transect may not necessarily be perpendicular to the wind. The receptor altitude ( $z$  in Eq. 1) is fixed at 2.5m, the height of the instrumentation above the road. Unless measured on site, meteorological data including wind speed, and stability are taken from NOAA's Ready Archived meteorology (<https://www.ready.noaa.gov>). These data are available in 3-hour increments and are interpolated to 1 hour data for use in the model. The hourly data are matched to the closest observation based on time. The stability data are used to identify the proper  $z$  and  $y$  dispersion parameters based on Briggs (1973) for rural areas.

As discussed in Sect. 1.1, the comparison between the observations and modeled output along a downwind transect is used to calculate emission rate. First, Eq. 1 was solved for the  $x$  and  $y$  measurement points using a reference emission rate ( $Q_{ref}$ ) taken to be  $1 \text{ kg s}^{-1}$  for simplicity. A comparison of observations and model output (using the reference emission) from 21 downwind transects is shown in Fig. 2. Note that the roads were not necessarily perpendicular to the wind, therefore the superposition of the plume on the roadway may not show a full Gaussian profile. Second, the observations and modeled concentrations were both integrated along  $y$  (summed since they consist of discrete points). Finally, because the concentrations scale linearly with the emission rate according to Eq. 1, the emission rate can be estimated as shown in Eq. 2.

$$Q = \frac{\sum C_{Observation}}{\sum C_{Model}} \times Q_{ref} \quad (2)$$

Where  $\Sigma$  implies summation. This method, with integrated concentrations, has the advantage of not relying on regressions between the instantaneous data and model data which may have very low correlation as the instantaneous plume is not expected to mirror a Gaussian profile on such a short time scale.

### 2.4 Large-Eddy Simulation

Large-eddy simulation (LES) is used to simulate the dispersion of CH<sub>4</sub> for sites that had been sampled with a tower for approximately 1 hour and sampled with the mobile lab with at least 10 transects at both the beginning and end of the observation period. The LES turbulent modeling technique is the most suitable for high Reynolds number flow and dispersion in the atmospheric boundary layer. The LES code used in this study has been widely validated (Bou-Zeid, Meneveau, and Parlange, 2005; Tseng, Meneveau, and Parlange, 2006; Li et al., 2016). Briefly, the LES code solves the resolved continuity, Navier-Stokes, and scalar conservation equations on a Cartesian grid, and models the unresolved motions using the Lagrangian scale-dependent dynamic subgrid-scale model (Bou-Zeid, Meneveau, and Parlange, 2005). The sharp interface (Mittal and Iaccarino, 2005) immersed boundary method is used to simulate flow with the presence of large solid structures (e.g. tanks in this study) in the field (Chester, Meneveau, and Parlange, 2007; Li, Bou-Zeid, and Anderson, 2016; Tseng, Meneveau, and



Parlange, 2006). Volumetric scalar sources are located on top of the structures or at other points around the source structure if needed to simulate the gas emissions. A pseudo-spectral method is used for horizontal spatial derivatives and second-order finite difference method is used for vertical spatial derivative with the needed treatments to overcome the Gibbs phenomenon following Li, Bou-Zeid and Anderson (2016). Second-order Adams-Bashforth method is used for time integration. The inflow velocity is a turbulent logarithmic profile generated from a separate simulation over homogeneous flat terrain. The inflow scalar is kept at a constant background concentration.

In total, 5 sites were simulated. Most sites were set up with 1 or 2 m horizontal and vertical grid resolution with total simulation domain size of 256 m in x (along-wind) and y (cross-wind) directions and 100 m in z (vertical) direction. Site 5, the controlled release, was set up with 1 m horizontal resolution and 0.2222 m vertical resolution with a full z dimension of 33.33 m; this was done to improve resolution of a source at low elevation. Site layouts are shown in Fig. 3. Sites were simulated for at least 30 min to allow the simulated turbulence to reach steady state. LES output is rescaled with the measured friction velocity and the scalar flux rate imposed in the simulation (i.e. to get a LES  $Q_{\text{ref}} = 1 \text{ kg s}^{-1}$ ) to allow direct comparison to the Gaussian model estimates. Table S1 summarizes conditions and domain parameters for all 5 sites. Sites were primarily selected for simple geometry with flat terrain and homogeneous upwind conditions. Generally, elevation differences across the domains were less than 4 m and structures could be easily seen and photographed from the road to aid in site set-up.

### 3 Sampling Strategy

#### 3.1 Model-Based Design of Sampling Strategy

As the LES output represents the best estimate for the ‘truth’ of how a plume evolves in a turbulent environment, a useful extension of the LES analysis would be to examine the output as a reference case to understand how ‘sampling’ the model environment by taking instantaneous ‘measurements’ of the concentration fields affects emission retrievals. The turbulent structures that LES can resolve are illustrated in Fig. 4, which contrasts instantaneous plumes and averaged plumes in both the horizontal stream-wise (x-y) and vertical cross-wind (y-z) perspective. To optimize sampling there are two important variables (1) the number of measurements and (2) the time interval between measurements. Increasing the number of measurements is expected to increase the accuracy of the retrieval; however, the time interval may also affect results as measurements with short spacing may sample similar coherent plume structures.

Using the LES output, random samples were picked from 1-N samples (N being the total number of available samples for a given scenario) with time intervals of 30s, 1 min, 2 min and random. These ‘transects’ were then integrated to replace  $C_{\text{observation}}$  in Eq. 2 and the average LES profile was used as  $C_{\text{Model}}$  to produce an emission rate. As shown in Fig. 5 (a-h) the effect of increasing the number of measurements clearly reduces the range of retrievals, but the benefits of adding transects slow down around 10 samples beyond which increasing the number of transects reduces the retrieval scatter very slowly. The 5-95% range of observations for percent difference (pd) decreases by 60% at 10 transects, but only decreases by an additional 10% by extending up to 70 transects. The 5-95% range of observation for relative standard deviation (rsd) follows a similar



but less extreme pattern with the range of observations decreasing by 20% up to 10 transects and decreasing by an additional 15% by extending up to 70 transects. Additionally, retrievals with 30s spacing (c-d) show increased bias as even high numbers of samples may measure plume structures that are similar as indicated by the low scatter, but are not very representative of the whole simulation. However, the 1 min (e-f), 2 min (g-h) and random (a-b) intervals look very similar indicating a 1 min interval can be used as a practical lower limit (this might somewhat depend on turbulence intensity and stability in the atmosphere however). Notably, the random sample shows an rsd of ~25% even at the maximum number of measurements (N). This confirms that there is variability expected simply due to atmospheric variability. Atmospheric variability may have many sources; in these simulation variability is attributed to turbulence. However, in a real dynamic environment atmospheric variability could also include effects of mean wind flow change and plume meandering, especially in low wind speed conditions (Vickers et al., 2008, Mortarini et al., 2016). These results indicate that in order to sample such that the measurements reflect the actual variability in the atmosphere, sites must be sampled with at least 10 transects with >1 min spacing.

### 3.2 Field Implementation

Field measurements were designed to target neutral stability found in the morning and evening with each sampling outing typically lasting four hours. Most sites were sampled 1-3 times (denoted as standard sampling), occasional sites were sampled with ~10 transects (replicate sampling) and a few sites were sampled with >10 transects as well as a tower (intensive sampling). Typically 2 replicate sampling sites were picked per outing to capture atmospheric variability for a given condition. The goal of the sampling strategy was to produce 1000 standard sampling sites, 100 replicate sampling sites and 10 intensive sampling sites. This was based upon the approximate amount of time to acquire each sample.

Field campaigns were deployed in the Marcellus shale spanning northeast and southwest Pennsylvania. In the end 940 well pads were sampled with standard sampling, 53 with replicate sampling and 17 sites with intensive sampling. These replicate sampling sites were generally chosen at the beginning and end of each sampling period to observe changes in variability that may be due to changes in atmospheric conditions. For standard sampling sites with multiple passes, the average rsd of emissions was 67% and the average maximum percent difference was 58%. The average rsd of emissions for the replicate sampling sites was 77% and the average maximum percent difference was 150%. The rsd ranged from 12% to 260%. These results are consistent with the LES results shown in Sect. 3.1 predicting small numbers of transects will yield an artificially low rsd and more transects are needed to produce an accurate measure of variability. While there is a large range in the rsd observed, ~75% had rsd values less than 100%.



## 4 Source Strength Determination

### 4.1 Source Strength Determination Strategy

Comparisons between the IGM calculated emission rates and LES output should be done with care because the LES cannot be scaled to different distances and wind angles easily. In addition, the base scenario for the Gaussian approach at all standard sites assumes there is only one source at the 1 m well-head location because the well-head is the only geolocated structure in a public database and is the only structure common at every site. Sites may have varying numbers of well-heads, but they are generally very close together (<10 m) so a centralized point is used for sites with multiple well heads. However, the Gaussian can in fact be adjusted to include multiple sources and source heights. In order to ensure that the differences between outputs are due to the calculated model diffusion and not differences in model set-up, we compare three scenarios: (i) the base scenario is the IGM approach used for all sites that assumes there is a single source at the well-head at 1 m (SS Gaussian), (ii) the second scenario assumes the sources are other structures on the domain (i.e. storage tanks and processing equipment) that are taller and uses a multi-source Gaussian (MS Gaussian) model and (iii) the LES that simulates sources at the same locations and heights as the MS Gaussian. A schematic of the source determination strategy is shown in Fig. 7.

To compare to the LES results, the observations were indexed to coordinates on the 256 by 256 m horizontal LES grid. The resulting transects were interpolated within the range of observations to account for grid cells with multiple data points or missing data points. The LES time series spanning ~30 minutes were averaged to produce a pseudo Gaussian distribution excluding a ~5 min warm up time. LES statistics (mean and std. dev. of scalar and wind components) were plotted as a function of time to determine the onset of a steady state (Fig. S2). The LES output was scaled according to Eq. 3 where  $M$  is the mass introduced into the simulation and  $u_*$  is the tower-observed friction velocity. For some sites the LES generated winds did not match observations (due to various potential input error sources such as surface roughness), so an additional correction factor was applied to the retrieved emissions as shown in Eq. 4. The prime indicates corrected values and the corrected wind speed comes from averaged tower observations. The peaks of the interpolated observations were centered to align with the peak location of the LES average plume as shown in Fig. 8; LES does not replicate the small changes in wind direction that can occur in the real-world (unless they are known and imposed). The LES scaled concentration at 3 m (the mobile lab measurement height) was treated as  $C_{\text{Model}}$  in Eq. 2 to produce LES derived emission rates. This methodology is used to calculate the LES emissions shown in Sects. 4.2 and 4.3.

$$C_{LES}^S = \frac{C_{LES}}{M u_*} \quad (3)$$

$$Q'_{LES} = \frac{u'_{LES}}{u_{LES}} Q_{LES} \quad (4)$$

### 4.2 Controlled Release

The controlled release experiment (Site 5) utilized 3 leak rates: 0.97 kg hr<sup>-1</sup>, 0.22 kg hr<sup>-1</sup> and 0.09 kg hr<sup>-1</sup>. Due to the low height of the release, the LES domain was modified to have vertical resolution of 0.2222 m with a total domain height of



33.33m. Boxplots of emission retrievals from three scenarios are shown in Fig. 9 and statistics are summarized in Table 2. The two Gaussian retrievals compare using NOAA winds, which is the base scenario for all sites, and using the in-situ measured wind. Since the controlled release used one release point, there is only one source at a known height and the SS Gaussian approach is used. The agreement increases greatly using the in-situ wind data as NOAA overestimated the winds during the latter two release rates.

The Gaussian approach with in-situ measured wind agrees quite well with the release, surprisingly better than the LES. This may be due to effects of stability the Gaussian can account for, but were not simulated in the LES where neutral conditions were assumed; this will be further discussed in Sect. 5.1. In this case the conditions shifted from slightly unstable to neutral during the second release, with the friction velocity (an important scaling parameter for LES) decreasing from 0.21 m s<sup>-1</sup> to 0.10 m s<sup>-1</sup>. The slightly better performance of the Gaussian method in the experiment suggests that the correction factors for stability are at least as important an input as the direct calculation of diffusion in LES across a dynamic environment. While the LES investigation is useful to investigate sources of error induced by sampling strategy, a controlled release is the most direct way to detect sources of bias, which otherwise would not be apparent. In general, the close agreement across a range of release rates shows no apparent bias, with the results scattered low and high relative to the release rate. While LES can readily account for unstable or stable conditions, this would come at a large computational cost as multiple demanding simulations would be needed. The results here show that this is in fact not necessary, at least over flat homogeneous terrain, as the Gaussian model provides a comparable performance at a very small fraction of the modeling effort.

The controlled release was also used as an observational constraint to investigate the sampling strategy identified by the LES. This was done by randomly selecting an increasing number of transects from each release and comparing the averages. The results in Fig. 10 are in excellent agreement with the LES results pattern seen in Fig. 5 where the average converges beyond 10 transects. This reiterates the importance of the sampling protocol and also shows the range of results possible if only a limited amount of transects are used. During each release, even though a constant source is being emitted, a few (1-3) transects showed no observed plume whatsoever.

### 4.3 Field Sites

Comparison between means for sites 1-4 are shown in Table 3. Relatively good agreement is found between the LES emission retrieval and the SS and MS Gaussian approach for Sites 1-4. The range of emission retrievals vary within a factor of two with average differences of 44%. Due to the effort to standardize the comparison between all approaches by centering and correcting the observations, the difference in emission is entirely due to the difference in the dispersion each model produces. The Gaussian models assume stability corrected diffusion coefficients from Briggs (1973) while the LES makes no assumptions and allows turbulence to be numerically solved. The LES, however, was only run under neutral stability in this study. As shown in Fig. 11, the horizontal dispersion generally matches well between the LES and the MS Gaussian, while the vertical dispersion exhibits slightly different behavior. In the sites studied the LES predicts peak flux at lower altitudes closer to the source and at higher altitudes farther from the sources with the equivalence point around 100 m (additional figures of



Gaussian and LES dispersion are shown in Figures S3-S5). The differences are due to the distance scaling in the Briggs (1973) model being different from the LES. While there are other analytical models for distance specific dispersion coefficients, the Briggs 1973 actually matches the LES profiles better across the range of sites explored here than several other common models (Gifford, 1976, Smith, 1968; see Figures. S6-S9). Vertical dispersion is generally more important than the horizontal dispersion as integrating across a transect will effectively nullify any differences resulting from horizontal diffusion. However, if a difference in vertical dispersion exists, this can drastically change the retrieved emission rate. Without observations at multiple heights, it is impossible to verify which assumption is correct. In the range of distances investigated in this study (<200 m) the overall discrepancy is small.

## 5 Uncertainty Analysis and Discussion

### 10 5.1 Other Uncertainty Sources

For this analysis, we have assumed the source to be constant during the time span of the measurements (typically 1 hour). This may not be true for all sites and may be a driver of variability. Regardless, we assume that source emission variability at this scale should be treated as measurement variability as it is not clear that there is a reason to quantify emission variability at scales less than 1 hour. Other sources of uncertainty we have investigated and found to be negligible include source location and source height in most cases. While well pads can be a few thousand m<sup>2</sup> in area, infrastructure that could generate leaks is usually clustered such that observed potential sources span a range of 50 m. Source locations were changed for Sites 1 and 2 as shown in Table 4 according to the location of potential sources including a wellhead (1), a gas processing unit (2) or a storage tank (3) and the resulting emission retrieval were compared. Changing the across-wind location has virtually no effect on emission retrieval, while changing the along-wind location can potentially change the emissions. This can be investigated theoretically by comparing the expected model sum as a function of distance assuming a 50 m shift in source location as shown in Fig. S10. This scenario assumes typical conditions observed in this dataset (3 m receptor height, 1.5 m s<sup>-1</sup> wind and neutral stability). Generally, changing the along-wind location of the sources changes the emission retrieval by less than 35% when measuring at >100 m downwind. However, at closer distances where the uncertainty in source location is on the order of the downwind distance this could be a major source of error. For reference, the median distance between observation and sources in this dataset is about 200 m with no sites closer than 30 m and only 5 sites less than 50 m. We also investigated the sensitivity of source height, which we estimate ranges from 1 m for wellheads to 8 m for some large storage tanks, as shown in Fig. S11. The results indicate that source height variation changes the emission retrieval by less than 15%, again due to the large distance from the source.

Additionally, as shown in Sect. 4.1, inaccurate wind data can be a potential source of error. Because the modeled CH<sub>4</sub> concentration scales with wind in both the Gaussian and LES models, uncertainty in this parameter is necessary to constrain. In the context of this analysis, we compared the NOAA wind to tower measurements of winds at 18 tower sites. NOAA wind speeds differed from the tower data on average by 50%. Given the linear relationship between the inverse of wind speed and



Q in the Gaussian equation (Eq. 1), uncertainty in the wind speed should produce the same magnitude uncertainty in the emission rate.

The final additional source of uncertainty investigated pertains to stability. The stability class determines the analytical equation used to derive the diffusion coefficients, thus affecting the emission rate. By again comparing a theoretical case, the effect of changing the stability class can be seen in Fig. S12. Making the stability class less stable will decrease the modeled concentration and consequently increase the emission retrieval while making the stability class more stable will have the opposite effect. The magnitude of the difference between consecutive stability classes is relatively consistent, averaging 40%.

Not investigated here, but potentially very important to uncertainty, is the effect of terrain including both non-uniform slopes and structures such as trees. In this analysis we have intentionally sampled sites that were determined to be relatively flat and open. All of the sites modelled in this study follow this criteria, even though not every site in our sample is as simple. The geometric mean of the absolute terrain slope for all of our ~1000 sampled sites was 3% and ~60% of the sites sampled had an absolute terrain slope of less than 5%. Nevertheless, some sites did contain more complex topography that could cause drastically different dispersion parameters. Such sites would need to be analyzed on a case by case basis as dispersion over complex topography is usually not generalizable because every site is unique (e.g. the inverse Gaussian modeling approach might work very well at one site but poorly at another). This analysis would be non-trivial and requires high resolution topography data, surface heat flux fields and many other inputs for accurate modelling. Another possible pathway to fully investigate the effects of terrain is to investigate correlation between site emissions determined using Gaussian models and terrain slope. From these analyses one can determine screening criteria to preserve data quality and examine the skill of Gaussian models over complex terrain in general. This is the subject of forthcoming work using the larger dataset and not discussed here.

## 5.2 Total Uncertainty Estimate

The sources for uncertainty and bias in the Gaussian measurements discussed in this analysis are summarized in Table 5. These include the uncertainty in the Gaussian diffusion constant by comparing to LES calculated diffusion, uncertainty due to source location and height and uncertainty due to wind speed and stability class. In addition, the LES was used to observe bias in the Gaussian derived concentration distributions and the controlled release was used to evaluate bias in both the Gaussian and LES results. Finally, the LES was used to determine the optimum sampling pattern to constrain actual atmospheric variability. The largest contributor to total uncertainty is atmospheric variability. As atmospheric variability is impossible to separate from other sources of uncertainty, such as wind speed, it is not surprising that it is the largest source of uncertainty. As described in Sect. 3.1, the LES derived atmospheric variability (defined as the standard deviation of emissions retrieved) is expected to be ~25%, considerably less than the standard deviation observed directly since the LES can capture effect of turbulence, but not due to changes in the mean flow and meandering plumes which can contribute significantly to overall atmospheric variability (Vickers, Mahrt and Belusic, 2008, Mortarini et al., 2016). This is also the practical limit of



uncertainty for this method since other sources of uncertainty could be mitigated by better on-site measurements and source location detection, but some atmospheric variability is impossible to reduce. While the higher observed atmospheric variability may be partially explained by far more complex real world conditions leading to higher standard deviations, this also emphasizes the possibility that other sources of uncertainty are contained in this realization of atmospheric variability. For instance most sites, while relatively flat, still have some inhomogeneous terrain that can influence and deflect wind or lead to increased turbulence. To combine the remaining sources of error a Monte Carlo simulation of errors through the Gaussian equation was performed. This approach was determined to be the most appropriate as opposed to adding in quadrature as uncertainties may not be normally distributed and emissions are constrained to be above zero, causing a skew to the emission retrievals. The combined effects produce a skewed distribution with a standard deviation of 100%. As discussed in Sect. 5.1, this analysis focuses on relatively flat, simple sites and is not intended to be generalized to extremely complex sites. We caution that the plume diffusion uncertainty is therefore a minimum expected value and could be a major source of uncertainty for very complex sites not investigated here.

### 5.3 Uncertainty through Different Averaging Approaches

One additional consideration is the method used to average transects to derive an emission estimate. We have chosen to average the emissions deduced from individual transects. Alternatively, the multiple transects themselves could be averaged to produce a single emission estimate. The latter method should theoretically be more Gaussian in shape and more comparable to the model, but requires enough transects to produce a Gaussian profile and may not be appropriate for sites with a limited number of transects. However, we analyzed a representative site as a comparison to provide information as to what, if any, difference in retrieved emissions may be expected with this method. As an example, Site 3 was chosen to average the multiple transects previously shown in Fig. 2. The averaged plume, shown in Fig. 12, was then used to calculate the emission rate using the IGM approach, also using the model averaged across all transects. The averaged transect emission rate is  $1.2 \text{ kg hr}^{-1}$ , extremely close to the  $1.1 \text{ kg hr}^{-1}$  average of all single transects. The single transects range from passes with no plume detected to a maximum of  $2.6 \text{ kg hr}^{-1}$ .

Averaging multiple transects has the benefit of reducing the influence of atmospheric variability on the uncertainty of the measurement; however, longer measurement time is still required due to the need for many transects. Each approach, averaging emissions vs. averaging transects, produces similar final results indicating that averaging method is not a driver of emission uncertainty. Either approach may be acceptable given the constraints and intent of a sampling session. The variability of single transects of emissions may be a useful tool for data quality control while averaged transects may be useful in additional analysis intent on pinpointing the location of an unknown source.

### 5.4 Advantages and Disadvantages

Of the approaches compared in this analysis, the LES results require far more computational and processing time. Though inputs can be estimated from other sources (i.e. NOAA), we chose to measure meteorological variables directly which



contributed to significantly longer measurement time. While this should be considered best practice when producing computationally expensive LES outputs, there are no inherent differences between inputs needed for LES and Gaussian approaches and the Gaussian approach also benefits from on-site measurements making in-field measurement time theoretically similar. In practice, the additional set-up time for meteorological instrumentation can increase total measurement time for sites intended for LES to >1 hour. Table 6 summarizes main advantages and disadvantages for each technique. The main advantage of the LES is the ability to directly calculate the plume diffusion rather than rely on simplified models. However, the LES simulations shown here have all been initialized for neutral conditions, which is the stability class we targeted during sampling. This is a relatively transient atmospheric phase typically only occurring in the morning and evening around sunrise and sunset and generally other stability classes are encountered. The Gaussian method enables easy corrections for different stabilities allowing quick processing of data collected in these regimes. While LES can be programmed with different stabilities, the additional computational cost is great and the system energy change must be known which introduces another source of uncertainty as actual heat fluxes may vary over the domain of interest and single point measurements may not be accurate. For these reasons, LES alone would not be the recommended method of calculating emission rates based on our study. Likewise, the single transect method, though fast, has many sources of uncertainty. Hence, the combination of all of these approaches described in Sect. 3 is expected to maximize sampling efficiency while minimizing uncertainty.

## 6 Comparison to Previous Uncertainty Estimates

Overall, we find LES to be a useful tool to examine Gaussian sampling strategy and sources of uncertainty for mobile laboratory measurements. Subsampling the LES output generates an optimum sampling pattern of at least 10 transects per site to obtain reliable statistics of measurement uncertainty due to atmospheric variability, which is the largest source of uncertainty. When sampling at distances greater than 150 m downwind of sites, the uncertainty due to source location and height are generally less than 20% (for cases where source location is known within 50 m and source height is known within 10 m). Using the LES and a controlled release, we confirm that the Gaussian model performs well and no sources of bias using our approach are observable. LES is therefore not required for studies where source strength calculation is the main goal. The emission retrievals generally fall within a range of two. From this we use Monte Carlo analysis to extrapolate that the 95% confidence interval for sites with standard sampling ( $n=2$ ) ranges from  $0.05x-6.0x$  where  $x$  is the emission rate. Using the same approach, sites that had multiple passes and wind measurements (replicate/intensive) can be further constrained to  $0.07x-2.5x$ . This uncertainty estimate is higher than Lan et al. (2015) who reported  $0.5x-1.5x$  at the 95% confidence interval. Their study is identical to the theoretical lower limit of uncertainty we calculate by assuming only the LES predicted atmospheric variability of 25%. It should be noted that Lan et al. (2015) did incorporate some averaging over a time frame of >10 min to their measurements which, as discussed in Section 5.3, can also decrease uncertainty. However, this would not mitigate all other sources of error previously discussed.



In addition, our standard sampling uncertainty range is greater than other Gaussian approaches with controlled releases which reported  $0.28(x) - 3.6(x)$  and  $0.334(x) - 3.34(x)$  (Rella et al., 2015, Yacovitch et al., 2015); the uncertainty range of the multi-transect sites studies here was similar in magnitude. However, their analysis did not account for additional sources of uncertainty (source location, stability, wind speed) which can result in uncertainties larger than the reported values.

5 As described in Sect. 3.2, the observed atmospheric variability can range from 10-200% meaning that in-situ observations of variability and post screening out conditions with unacceptably high variability may be a viable way to reduce uncertainty. Other factors such as wind speed and stability can have a strong effect and can be quantified to reduce uncertainty.

## 7 Recommendations

10 While the uncertainty derived for mobile Gaussian techniques is large compared to many other techniques discussed in Sect. 1, it is low enough to reliably separate ‘normal emissions’ from ‘extreme emissions’ that are orders of magnitude larger. Many emission sources exhibit lognormal distributions where this condition is met, making sampling a reliable way to identify extreme emission sites. However, longer sampling time, reliable mobile wind sampling and visualization of plume distributions are needed to feasibly constrain this method to under 50% for routine measurements. In summary, to facilitate more constrained uncertainty from other mobile platform based Gaussian emission estimates we recommend the following:

- 15 1. Sites should be isolated to reduce contamination from other sources and be accessible from thoroughfares at least 100 m away.
2. On-site wind measurement should be collected whenever possible.
3. Additional data be collected such as photographs (used here) or IR imagery to precisely locate the sources whenever possible.
- 20 4. Ideally, all sites should use  $\geq 10$  sampling transects to reliably measure atmospheric variability.
5. For experiments where sampling frequency is at a premium, at least 1 site per sampling outing should be repeated with  $\geq 10$  sampling transects to reliably measure atmospheric variability.
6. Uncertainty analysis should be a systematic part of Gaussian sampling design.
7. In the absence of other experiments to study measurement uncertainty (controlled releases), the repeat measurements  
25 may be a suitable approximation for the *minimum* expected uncertainty.
8. While the strategy described in the study was developed for well pads, the findings are generalizable to other ‘point-like’ sources ( $<2,500 \text{ m}^2$  and  $>100 \text{ m}$  downwind) with simple terrain.



## 8 Data Availability

The dataset for this publication is available upon contacting the corresponding author.

## 9 Author Contributions

D.R.C, Q.L. and E.B.Z. implemented LES modeling for sites. D.R.C, J.M.L and H.M.L. analyzed raw data and provided Gaussian fluxes. D.R.C., J.M.L, H.M.L, J.P.F., B.B., L.M.G., X.G., J.M., D.P., L.W., and M.A.Z. collected in-situ data. D.R.C, L.M.G., J.F.P., E.B.Z. and M.A.Z. assisted in sampling design. L.M.G, D.P., B.B. and X.G. provided technical support for data collection and instrument integration. J.M. provided mechanical assistance in mobile lab design and deployment. D.R.C prepared the manuscript with feedback from all authors.

## 10 Competing Interests

10 The authors declare that they have no conflict of interest.

## 11 Acknowledgements

We would like to thank all members of the fieldwork team including Stephany Paredes-Mesa, Tanvir Mangat and Kira Olander. We would also like to thank Maider Llaguno Munitxa for her help with the mobile tower modeling. We thank LICOR Biosciences for lending instrumentation used in this campaign. This work was funded by NOAA CPO/AC4,  
15 #NA14OAR4310134.



## 12 References

- Allen, D. T., Torres, V. M., Thomas, J., Sullivan, D. W., Harrison, M., Hendler, A., Herndon, S. C., Kolb, C. E., Fraser M. P., Hill, A. D., and Lamb, B. K.: Measurements of methane emissions at natural gas production sites in the United States, *P. Natl. Acad. Sci. U.S.A.*, 110, 17768-73, doi: 10.1073/pnas.1304880110, 2013.
- 5 Allen, D. T., Pacsi, A. P., Sullivan, D. W., Zavala-Araiza, D., Harrison, M., Keen, K., Fraser, M. P., Hill, A. D., Sawyer, R. F., and Seinfeld, J. H.: Methane emissions from process equipment at natural gas production sites in the United States: Pneumatic controllers, *Envir. Sci. Tech.*, 49, 633-40, doi: 10.1021/es5040156, 2014.
- Baker, L. H., Collings, W. J., Olivie, D. J. L., Cherian, R., Hodnebrog, O., Myhre, G., and Quass, J.: Climate responses to anthropogenic emissions of short-lived climate pollutants, *Atmos. Chem. Phys.*, 15, 8201-8216, doi: 10.5194/acp-15-8201-2015, 2015.
- 10 Batchelor, G. K.: Diffusion in a field of homogeneous turbulence. I. Eulerian Analysis, *Aust. J. Sci. Res.*, 2, 437-50, doi: 10.1071/CH9490437, 1949.
- Bosanquet, C. H., and Pearson, J. L.: The Spread of Smoke and Gases from Chimneys, *Trans. Faraday Soc.*, 32, 1249-63, 1936.
- 15 Bou-Zeid, E., Meneveau, C., and Parlange, M.: A Scale-Dependent Lagrangian Dynamic Model for Large Eddy Simulation of Complex Turbulent Flows, *Phys. Fluids*, 17, doi:10.1063/1.1839152, 2005.
- Bowerman, N. H. A., Frame, D. J., Huntingford, C., Lowe, J. A., Smith, S. M., and Allen, M. R.: The role of short-lived climate pollutants in meeting temperature goals, *Nat. Clim. Change*, 3, 1021-24, doi: 10.1038/nclimate2034, 2013.
- Brantley, H. L., Thoma, E. D., Squier, W. C., Guven, B. B., and Lyon, D.: Assessment of methane emissions from oil and gas production pads using mobile measurements, *Envir. Sci. Tech.*, 48, 14508-15, doi: 10.1021/es503070q, 2014.
- 20 Briggs, G. A.: Diffusion estimation for small emissions, in environmental research laboratories, *Air Resources Atmospheric Turbulence and Diffusion Laboratory 1973 Annual Report*, USAEC Report ATDL-106, National Oceanic and Atmospheric Administration, 83-145, 1973.
- Caulton, D. R., Shepson, P. B., Santoro, R. L., Sparks, J. P., Howarth, R. W., Ingraffea, A. R., Cambaliza, M. O., Sweeney, C., Karion, A., Davis, K. J., and Stirm, B. H.: Toward a better understanding and quantification of methane emissions from shale gas development, *P. Natl. Acad. Sci. U.S.A.*, 111, 6237-42, doi: 10.1073/pnas.1316546111, 2014.
- 25 Foster-Wittig, T. A., Thoma, E. D., and Albertson, J. D.: Estimation of point source fugitive emission rates from a single sensor time series: A conditionally-sampled Gaussian plume reconstruction, *Atmos. Environ.*, 115, 101-9, doi: 10.1016/j.atmosenv.2015.05.042, 2015.
- 30 Frankenberg, C., Thorpe, A. K., Thompson, D. R., Hulley, G., Kort, E. A., Vance, N., Borchardt, J., Krings, T., Gerilowski, K., Sweeney, C., and Conley, S.: Airborne methane remote measurements reveal heavy-tail flux distribution in Four Corners region, *P. Natl. Acad. Sci. U.S.A.*, 113, 9734-39, doi: 10.1073/pnas.1605617113, 2016.



- Gålfalk, M., Olofsson, G., Crill, P., and Bastviken, D.: Making methane visible, *Nat. Clim. Change*, 6, 426-30, doi:10.1038/nclimate2877, 2016.
- Gifford, Jr., F. A.: An outline of theories of diffusion in the lower layers of the atmosphere, in: *Meteorology and Atomic Energy*, Slade, D. (Ed.), U.S. Atomic Energy Commission, TID-24190, Springfield, Virginia, 65-116, 1968.
- 5 Gifford, Jr., F. A.: Turbulent diffusion-typing schemes: a review, *Nucl. Safety*, 17, 68-86, 1976.
- Hilst, G. R.: The Dispersion of Stack Gases in Stable Atmospheres, *J. Air Pollut. Control Assoc.*, 7, 205-10, doi: 10.1080/00966665.1957.10467804, 1957.
- Kang, M., Kanno, C. M., Reid, M. C., Zhang, X., Mauzerall, D. L., Celia, M. A., Chen, Y., and Onstott, T. C.: Direct measurements of methane emissions from abandoned oil and gas wells in Pennsylvania, *P. Natl. Acad. Sci. U.S.A.*,
- 10 111, 18173-7, doi: 10.1073/pnas.1408315111, 2014.
- Karion, A., Sweeney, C., Pétron, G., Frost, G., Hardesty, R. M., Kofler, J., Miller, B. R., Newberger, T., Wolter, S., Banta, R., and Brewer, A.: Methane emissions estimate from airborne measurements over a western United States natural gas field, *Geophys. Res. Lett.* 40, 4393-7, doi: 10.1002/grl.50811, 2013.
- Karion, A., Sweeney, C., Kort, E. A., Shepson, P. B., Brewer, A., Cambaliza, M., Conley, S. A., Davis, K., Deng, A.,
- 15 Hardesty, M., and Herndon, S. C.: Aircraft-based estimate of total methane emissions from the Barnett Shale region. *Envir. Sci. Tech.*, 49, 8124-31, doi: 10.1021/acs.est.5b00217, 2015.
- Kirschke, S., Bousquet, P., Ciais, P., Saunois, M., Canadell, J. G., Dlugokencky, E. J., Bergamaschi, P., Bergmann, D., Blake, D. R., Bruhwiler, L., Cameron-Smith, P., Castaldi, S., Chevallier, F., Feng, L., Fraser, A., Heimann, M., Hodson, E. L., Houweling, S., Josse, B., Fraser, P. J., Krummel, P. B., Lamarque, J.-F., Langenfelds, R. L., Le
- 20 Quéré, C., Naik, V., O'Doherty, S., Palmer, P. I., Pison, I., Plummer, D., Poulter, B., Prinn, R. G., Rigby, M., Ringeval, B., Santini, M., Schmidt, M., Shindell, D. T., Simpson, I. J., Spahni, R., Steele, L. P., Strode, S. a., Sudo, K., Szopa, S., van der Werf, G. R., Voulgarakis, A., van Weele, M., Weiss, R. F., Williams, J. E. and Zeng, G.: Three decades of global methane sources and sinks, *Nat. Geosci.*, 6(10), 813–823, doi:10.1038/ngeo1955, 2013.
- Kort, E. A., Frankenberg, C., Costigan, K. R., Lindenmaier, R., Dubey, M. K., and Wunch, D.: Four corners: The largest US methane anomaly viewed from space, *Geophys. Res. Lett.*, 41, 6898-903, doi: 10.1002/2014GL061503, 2014.
- 25 Kuai, L., Worden, J. R., Li, K.-F., Hulley, G. C., Hopkins, F. M., Miller, C. E., Hook, S. J., Duren, R. M., and Aubrey, A. D.: Characterization of anthropogenic methane plumes with the Hyperspectral Thermal Emission Spectrometer (HyTES): a retrieval method and error analysis. *Atmos. Meas. Tech.*, 9, 3165, 2016.
- Lamb, B. K., Edburg, S. L., Ferrara, T. W., Howard, T., Harrison, M. R., Kolb, C. E., Townsend-Small, A., Dyck, W.,
- 30 Possolo, A., and Whetstone, J. R.: Direct measurements show decreasing methane emissions from natural gas local distribution systems in the United States, *Envir. Sci. Tech.*, 49, 5161-9, doi: 10.1021/es505116p, 2015.
- Lan, X., Talbot, R., Laine, P., and Torres, A.: Characterizing fugitive methane emissions in the Barnett Shale area using a mobile laboratory, *Envir. Sci. Tech.*, 49, 8139-46, doi: 10.1021/es5063055, 2015.



- Lavoie, T. N., Shepson, P. B., Cambaliza, M. O., Stirm, B. H., Karion, A., Sweeney, C., Yacovitch, T. I., Herndon, S. C., Lan, X., and Lyon, D.: Aircraft-based measurements of point source methane emissions in the Barnett Shale basin, *Envir. Sci. Tech.*, 49, 7904-13, doi: 10.1021/acs.est.5b00410, 2015.
- Li, Q., Bou-Zeid, E., and Anderson, W.: The Impact and Treatment of the Gibbs Phenomenon in Immersed Boundary Method Simulations of Momentum and Scalar Transport, *J. Comput. Phys.*, 310, 237–51, doi:10.1016/j.jcp.2016.01.013, 2016.
- Li, Q., Bou-Zeid, E., Anderson, W., Grimmond S., and Hultmark M.: Quality and Reliability of LES of Convective Scalar Transfer at High Reynolds Numbers, *Int. J. Heat Mass Transfer*, 102, 959–970, doi:10.1016/j.ijheatmasstransfer.2016.06.093, 2016.
- 10 Mortarini, L., Stefanello, M., Degrazia, G., Roberti, D., Castelli, S. T., and Anfossi, D.: Characterization of Wind Meandering in Low-Wind-Speed Conditions, *Bound.-Lay. Meteorol.*, 161, 165-82, doi: 10.1007/s10546-016-0165-6, 2016.
- Mittal, R., and Iaccarino, G.: Immersed Boundary Methods, *Annu. Rev. Fluid Mech.*, 37, 239–61, doi:10.1146/annurev.fluid.37.061903.175743, 2005.
- 15 Nathan, B. J., Golston, L. M., O'Brien, A. S., Ross, K., Harrison, W. A., Tao, L., Lary, D. J., Johnson, D. R., Covington, A. N., Clark, N. N., and Zondlo, M. A.: Near-field characterization of methane emission variability from a compressor station using a model aircraft, *Envir. Sci. Tech.*, 49, 7896-903, doi: 10.1021/acs.est.5b00705, 2015.
- Omara, M., Sullivan, M. R., Li, X., Subramanian, R., Robinson, A. L., and Presto, A. A.: Methane emissions from conventional and unconventional natural gas production sites in the Marcellus Shale Basin, *Envir. Sci. Tech.*, 50, 2099-107, doi: 10.1021/acs.est.5b05503, 2016.
- 20 Peischl, J., Ryerson, T. B., Brioude, J., Aikin, K. C., Andrews, A. E., Atlas, E., Blake, D., Daube, B. C., Gouw, J. A., Dlugokencky, E., and Frost, G. J.: Quantifying sources of methane using light alkanes in the Los Angeles basin, California. *J. Geophys. Res.-Atmos.*, 118, 4974-90, doi: 10.1002/jgrd.50413, 2013.
- Peischl, J., Ryerson, T. B., Aikin, K. C., Gouw, J. A., Gilman, J. B., Holloway, J. S., Lerner, B. M., Nadkarni, R., Neuman, J. A., Nowak, J. B., and Trainer, M. Quantifying atmospheric methane emissions from the Haynesville, Fayetteville, and northeastern Marcellus shale gas production regions, *J. Geophys. Res.-Atmos.*, 120, 2119-39, doi: 10.1002/2014JD022697, 2015.
- 25 Peischl, J., Karion, A., Sweeney, C., Kort, E. A., Smith, M. L., Brandt, A. R., Yeskoo, T., Aikin, K. C., Conley, S. A., Gvakharia, A., and Trainer, M.: Quantifying atmospheric methane emissions from oil and natural gas production in the Bakken shale region of North Dakota. *J. Geophys. Res.-Atmos.*, 121, 6101-11, doi: 10.1002/2015JD024631, 2016.
- 30 Pétron, G., Frost, G., Miller, B. R., Hirsch, A. I., Montzka, S. A., Karion, A., Trainer, M., Sweeney, C., Andrews, A. E., Miller, L., and Kofler, J.: Hydrocarbon emissions characterization in the Colorado Front Range: A pilot study, *J. Geophys. Res.-Atmos.*, 117, D04304, doi: 10.1029/2011JD016360, 2012.



- Pétron, G., Karion, A., Sweeney, C., Miller, B. R., Montzka, S. A., Frost, G. J., Trainer, M., Tans, P., Andrews, A., Kofler, J., and Helmig, D.: A new look at methane and nonmethane hydrocarbon emissions from oil and natural gas operations in the Colorado Denver-Julesburg Basin. *J. Geophys. Res.-Atmos.*, 119, 6836-52, doi: 10.1002/2013JD021272, 2014.
- 5 Ravikumar, A. P., Wang, J., and Brandt, A. R.: Are Optical Gas Imaging Technologies Effective for Methane Leak Detection?, *Envir. Sci. Technol*, 51, 718-24, doi: 10.1021/acs.est.6b03906, 2017.
- Ren, X., Hall, D. L., Vinciguerra, T., Benish, S. E., Stratton, P. R., Ahn, D., Hansford, J. R., Cohen, M. D., Sahu, S., He, H., and Grimes, C.: Methane Emissions from the Marcellus Shale in Southwestern Pennsylvania and Northern West Virginia Based on Airborne Measurements, *J. Geophys. Res.-Atmos.*, 122, 4639-53, doi: 10.1002/2016JD026070, 10 2017.
- Rella C. W., Tsai, T. R., Botkin, C. G., Crosson, E. R., and Steele, D.: Measuring emissions from oil and natural gas well pads using the mobile flux plane technique, *Envir. Sci. Tech.*, 49, 4742-8, doi: 10.1021/acs.est.5b00099, 2015.
- Roscioli, J. R., Yacovitch, T. I., Floerchinger, C., Mitchell, A. L., Tkacik, D. S., Subramanian, R., Martinez, D. M., Vaughn, T. L., Williams, L., Zimmerle, D., and Robinson, A. L.: Measurements of methane emissions from natural gas gathering facilities and processing plants: measurement methods, *Atmos. Meas. Tech.*, 8, 2017-35, doi: 10.5194/amt-8-2017-2015, 15 2015.
- Smith, M. E.: Recommended guide for the prediction of the dispersion of airborne effluents. ASME, New York, 1968.
- Subramanian, R., Williams, L. L., Vaughn, T. L., Zimmerle, D., Roscioli, J. R., Herndon, S. C., Yacovitch, T. I., Floerchinger, C., Tkacik, D. S., Mitchell, A. L., and Sullivan, M. R.: Methane Emissions from Natural Gas Compressor Stations in the Transmission and Storage Sector: Measurements and Comparisons with the EPA Greenhouse Gas Reporting Program Protocol, *Envir. Sci. Tech.*, 49, 3252-61, doi: 10.5194/amt-8-2017-2015, 20 2015.
- Sutton, O. G.: A Theory of Eddy Diffusion in the Atmosphere, *P. R. Soc. Lond. A-Conta.*, 135, 143-165, 1932.
- Tao, L., Sun, K., Miller, D. J., Pan, D., Golston, L. M., and Zondlo, M. A.: Low-power, open-path mobile sensing platform for high-resolution measurements of greenhouse gases and air pollutants, *Appl. Phys. B-Lasers O.*, 119, 25 153-64, doi: 10.1007/s00340-015-6069-1, 2015.
- Thorpe, A. K., Frankenberg, C., Aubrey, A. D., Roberts, D. A., Nottrott, A. A., Rahn, T. A., Sauer, J. A., Dubey, M. K., Costigan, K. R., Arata, C., and Steffke, A. M.: Mapping methane concentrations from a controlled release experiment using the next generation Airborne Visible/Infrared Imaging Spectrometer (AVIRIS-NG), *Remote Sens. Environ.*, 179, 104-15, doi: 10.1016/j.rse.2016.03.032, 2016.
- 30 Townsend-Small, A., Marrero, J. E., Lyon, D. R., Simpson, I. J., Meinardi, S., and Blake, D. R.: Integrating source apportionment tracers into a bottom-up inventory of methane emissions in the Barnett Shale hydraulic fracturing region, *Envir. Sci. Tech.*, 49, 8175-82, doi: 10.1021/acs.est.5b00057, 2015.
- Tseng, Y. H., Meneveau, C., and Parlange, M. B.: Modeling Flow Around Bluff Bodies and Predicting Urban Dispersion Using Large Eddy Simulation, *Envir. Sci. Tech.*, 40, 2653-62, doi:10.1021/es051708m, 2006.



- U.S. EPA: Other Test Methods (OTM) 33 and 33A Geospatial Measurement of Air Pollution-Remote Emissions Quantification Direct Assessment (GMAP-REQ-DA), <https://www3.epa.gov/ttnemc01/prelim/otm33a.pdf>, 2014.
- Veigle, W. J., and Head, J. H.: Derivation of the Gaussian Plume Model, *J. Air Pollut. Control Assoc.*, 28, 1139-40, doi: 10.1080/00022470.1978.10470720, 1978.
- 5 Vickers, D., Mahrt, L., and Belusic, D.: Particle simulations of dispersion using observed meandering and turbulence, *Acta Geophys.*, 56, 234-56, doi:10.2478/s11600-007-0041-3, 2008.
- Yacovitch, T. I., Herndon, S. C., Petron, G., Kofler, J., Lyon, D., Zahniser, M. S., and Kolb, C. E.: Mobile Laboratory Observations of Methane Emissions in the Barnett Shale Region, *Envir. Sci. Tech.*, 49, 7889-95, doi:10.1021/es506352j, 2015.
- 10 Zannetti, P.: *Air Pollution Modeling: Theories, Computational Methods, and Available Software*, Van Nostrand Reinhold, New York, U.S.A., 141-183, 1990.
- Zimmerle, D. J., Williams, L. L., Vaughn, T. L., Quinn, C., Subramanian, R., Duggan, G. P., Willson, B., Opsomer, J. D., Marchese, A. J., Martinez, D. M., and Robinson, A. L.: Methane emissions from the natural gas transmission and storage system in the United States, *Envir. Sci. Tech.*, 49, 9374-83, doi: 10.1021/acs.est.5b01669, 2015.
- 15 Zickfeld, K., Solomon, S., and Gilford, D. M.: Centuries of thermal sea-level rise due to anthropogenic emissions of short-lived greenhouse gases, *P. Natl. Acad. Sci. U.S.A.*, 114, 657-62, doi: 10.1073/pnas.1612066114, 2017.



## Tables

Table 1. Comparison of CH<sub>4</sub> emission measurement techniques and reported uncertainties.

Technique	Referenced Study	Reference Uncertainty Range*
Ground-Based Thermal Imaging	Gålfalk et al., 2016	3-15%
Aircraft Remote Sensing	Kuai et al., 2016, Frankenberg et al., 2016, Thorpe et al., 2016	5-20%
Satellite Remote Sensing	Kort et al., 2014	15%
Chamber Sampling	Allen et al., 2013 and 2014, Kang et al., 2014	20-30%
Ground-Based Tracer Correlation	Lamb et al., 2015, Roscioli et al., 2015, Subramanian et al., 2015, Zimmerle et al., 2015, Omara et al., 2016	20-50%
Aircraft/UAV Mass Balance	Karion et al., 2013 and 2015, Peischl et al., 2013, 2015 and 2016, Caulton et al., 2014, Pétron et al., 2014, Lavoie et al., 2015, Nathan et al., 2015, Ren et al., 2017	20-75%
Ground-Based Stationary Dispersion	Brantley et al., 2014, Foster-Wittig et al., 2015	25-60%
Tall Tower Monitoring	Pétron et al., 2012	50-100%
Ground-Based Mobile Dispersion	Lan et al., 2015, Rella et al., 2015, Yacovitch et al., 2015	50-350%

\* Uncertainty range reflects author reported uncertainty on *emission* numbers, not necessarily measurement uncertainty. Some author's specify a 95% confidence interval, others use 1 or 2 standard deviations and others compute upper and lower bounds.



Table 2. Summary of mean emissions from three scenarios for the controlled release ( $\pm 1\sigma$ ).

Scenario	Release 1 (kg hr <sup>-1</sup> )	Release 2 (kg hr <sup>-1</sup> )	Release 3 (kg hr <sup>-1</sup> )
Release Rate	0.97	0.22	0.09
No. of Transects	19	10	13
Gaussian w/ NOAA winds	0.97 ± 0.76	0.79 ± 0.40	0.35 ± 0.15
Gaussian w/ tower winds	0.72 ± 0.54	0.23 ± 0.12	0.10 ± 0.04
LES	0.94 ± 0.76	0.44 ± 0.20	0.22 ± 0.11



Table 3. Comparison of mean emission rates using three scenario from four sites ( $\pm 1\sigma$ ).

Scenario	Site 1 (kg hr <sup>-1</sup> )	Site 2 (kg hr <sup>-1</sup> )	Site 3 (kg hr <sup>-1</sup> )	Site 4 (kg hr <sup>-1</sup> )
SS Gaussian	1.0 ± 1.4	0.19 ± 0.14	1.08 ± 0.76	0.19 ± 0.26
MS Gaussian	2.2 ± 4.7	0.24 ± 0.31	1.8 ± 1.2	0.29 ± 0.27
LES	1.5 ± 2.2	0.18 ± 0.15	0.76 ± 0.50	0.18 ± 0.16



Table 4. Comparison of emissions for different source location scenarios.

Site	Scenario	Emission (kg hr <sup>-1</sup> )	Change in x distance (m)	Change in y distance (m)	Change in z distance (m)	Difference (%)
1	1	0.54	--	--	--	--
	2	1.33	40	0	1	150
	3	0.47	0	15	7	13
2	1	0.14	--	--	--	--
	2	0.15	58	49	1	7.5
	3	0.14	72	0	7	5



Table 5. Sources and magnitude of uncertainty.

Uncertainty Source	Notes	Expected Uncertainty
Atmospheric Variability	Requires $\geq 10$ transect to quantify, not independent from other uncertainty sources	77%
Instrumental Uncertainty	LI 7700 stated precision of 5 ppb	1%
Plume Turbulent Diffusion	Potentially source of uncertainty and bias	25%
Source Location	Combined x, y and z uncertainty low at distance $>150\text{m}$	15%
Stability	Potential 1 stability class discrepancy	40%
Wind Speed	Uncertainty scales linearly	50%
Total		100%



Table 6. Summary of advantages and disadvantages of each technique.

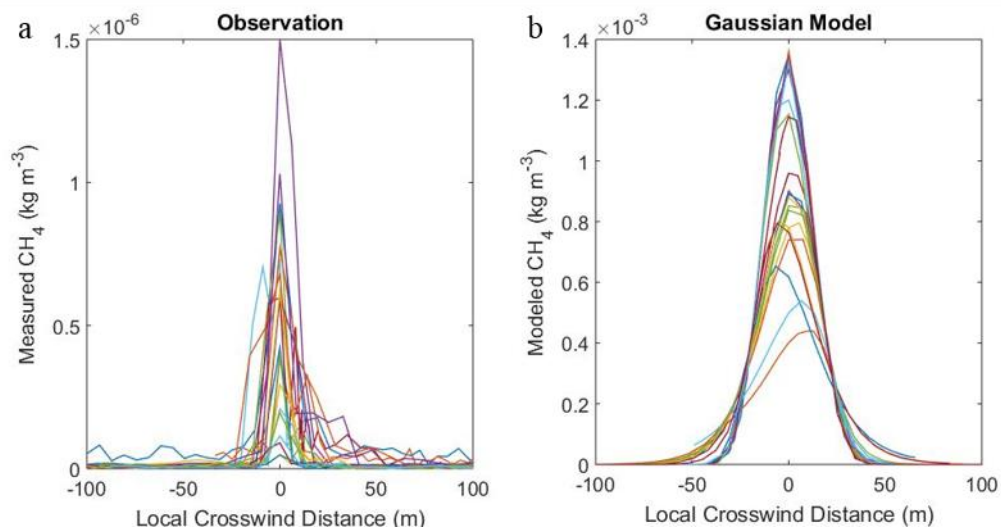
	Measurement Time	Processing Time	Sources of Uncertainty
Single Transect Gaussian	Short (<10 min)	Short (~few minutes)	Many sources, atmospheric variability unconstrained
Multi-Transect Gaussian	Moderate (15-30 min)	Short (~few minutes)	Atmospheric variability constrained, diffusion unconstrained
Multi-Transect LES	Moderate to Long (15 min-1 hr)	Very Long (several days)	Atmospheric variability constrained, diffusion constrained



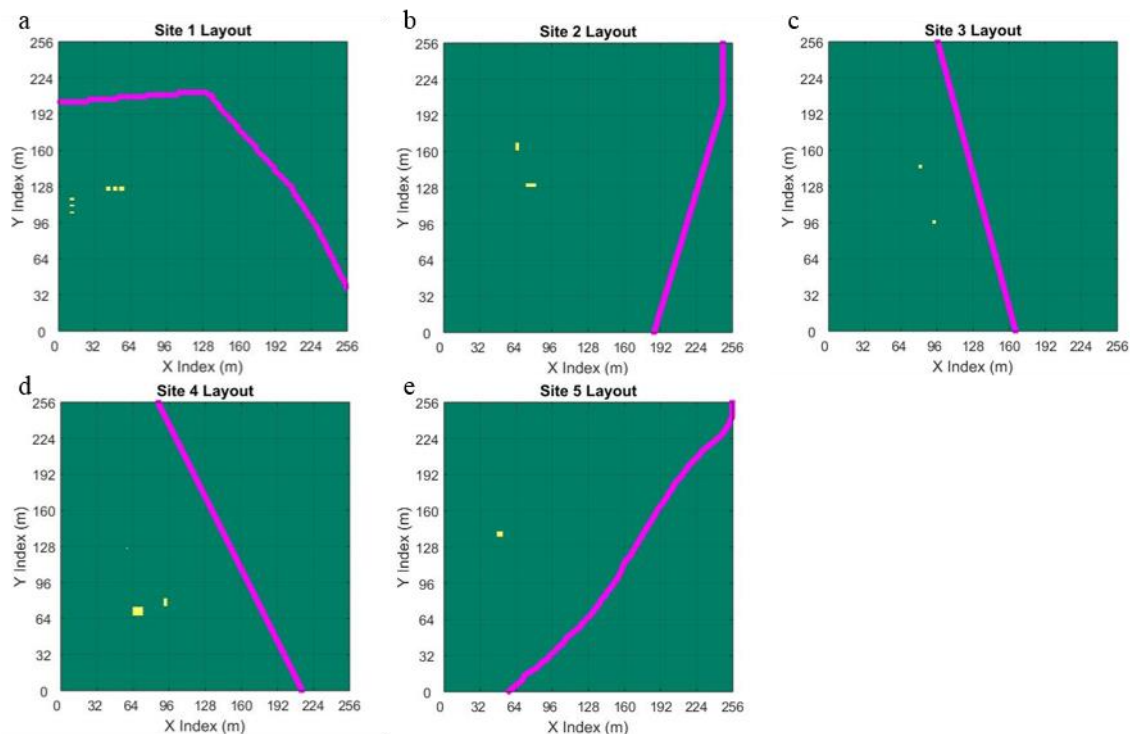
## Figures



Figure 1. (a) The Princeton atmospheric chemistry experiment (PACE), (b) close-up of PACE roof rack with  
5 instrumentation and (c) mobile tower platform.



**Figure 2. (a) Observations of CH<sub>4</sub> at a site showing multiple downwind transects and the local crosswind (y) distance. (b) Gaussian outputs along the same downwind transects.**



**Figure 3.** Site layouts showing emitting structures in yellow and the road in magenta for (a) Site 1, (b) Site 2, (c) Site 3, (d) Site 4 and (e) Site 5. For visibility the roads are shown thicker than reality.

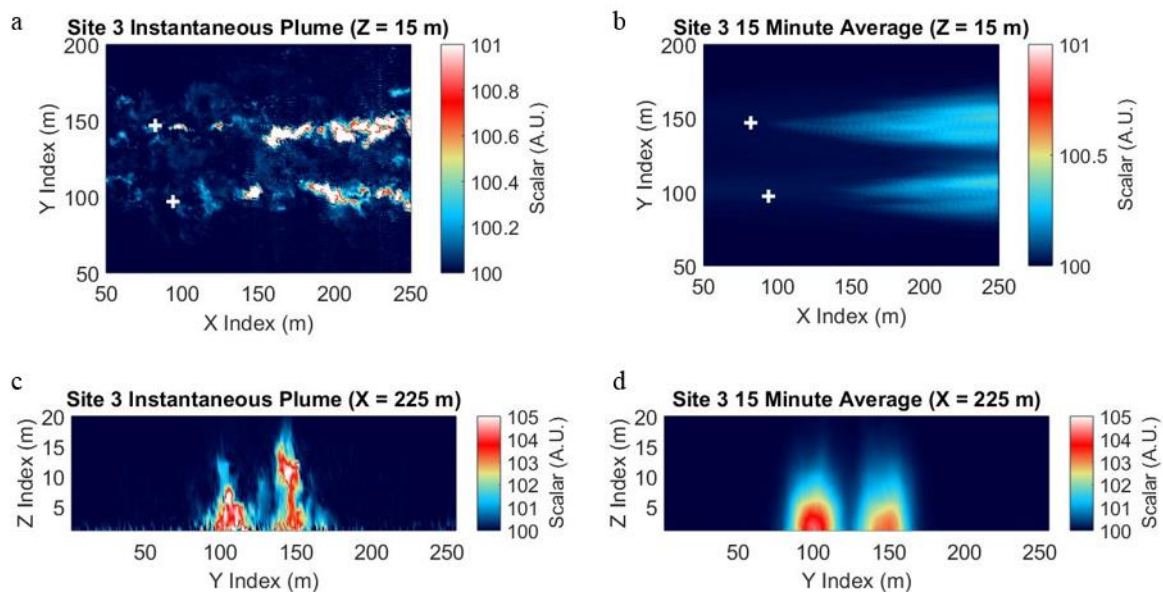


**Figure 4.** Comparison of instantaneous (a/c) and 15 min averaged (b/d) plume for Site 3. Panels a and b show scalar with arbitrary units (A.U.) in a x-y cross section at an altitude of 15 m and panels c and d show a x-z cross section at a 225 m downwind distance. The release locations are shown with a white marker (+).

5

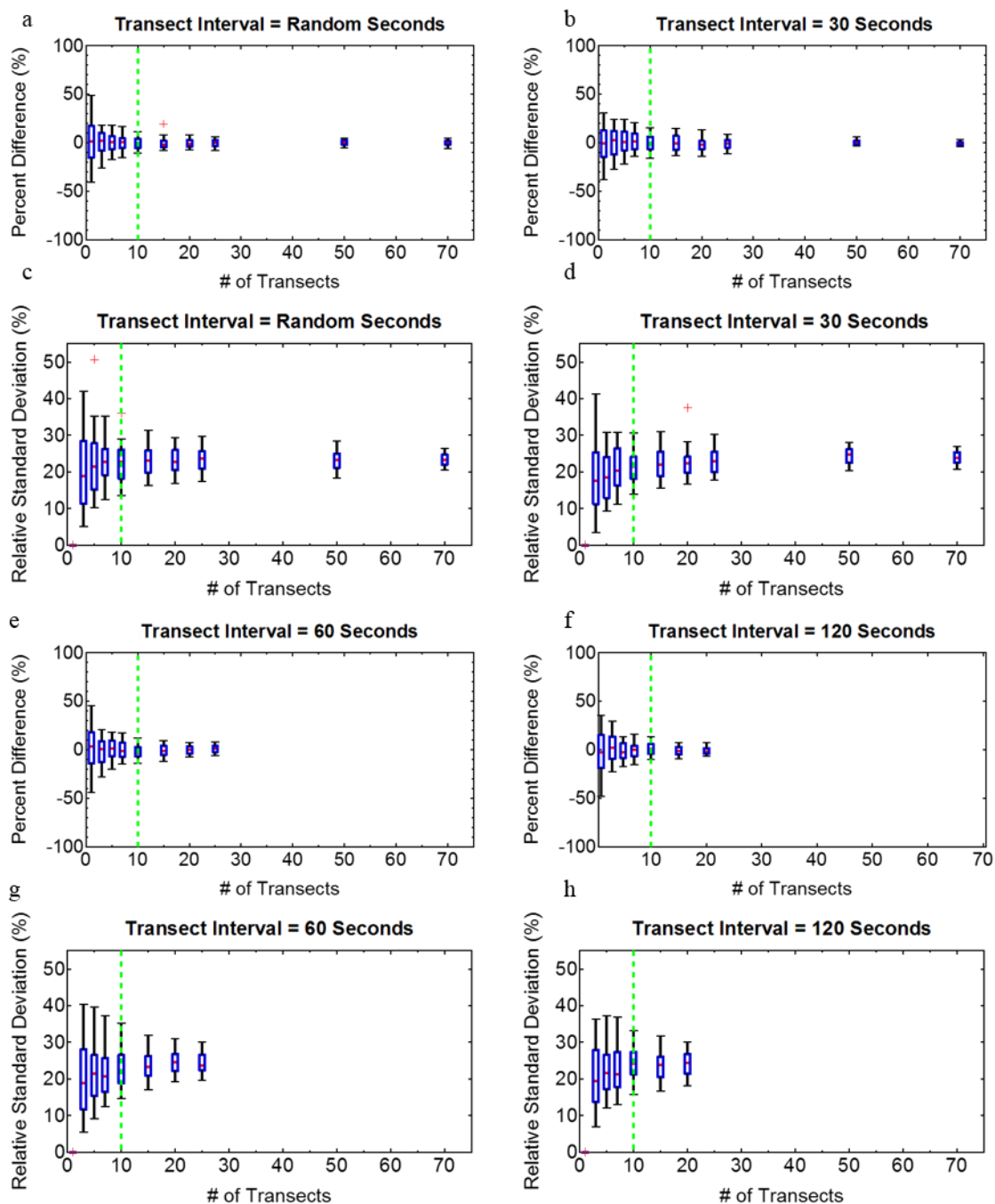


Figure 5. The percent difference (a,b,e,f) between emission retrieval and known simulation emission rate and rsd (c,d,g,h) of the emission retrieval using various amounts of transects and random (a,c), 30 second (b,d), 1 minute (e,g) or 2 minute (f,h) transect spacing. Box and whiskers plots show the 50% percentile (red), 25 and 75% percentile (blue) and 10 and 90% percentile (black). The recommended 10 transect criteria is shown in green.

5

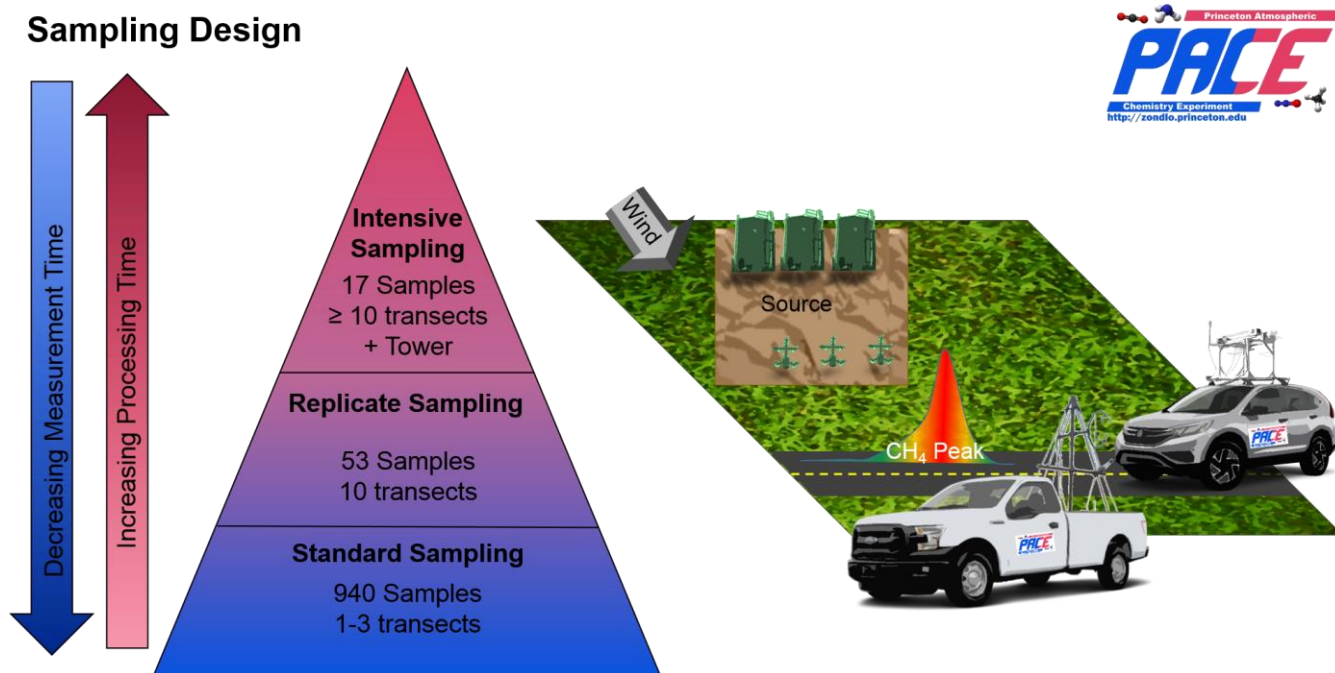
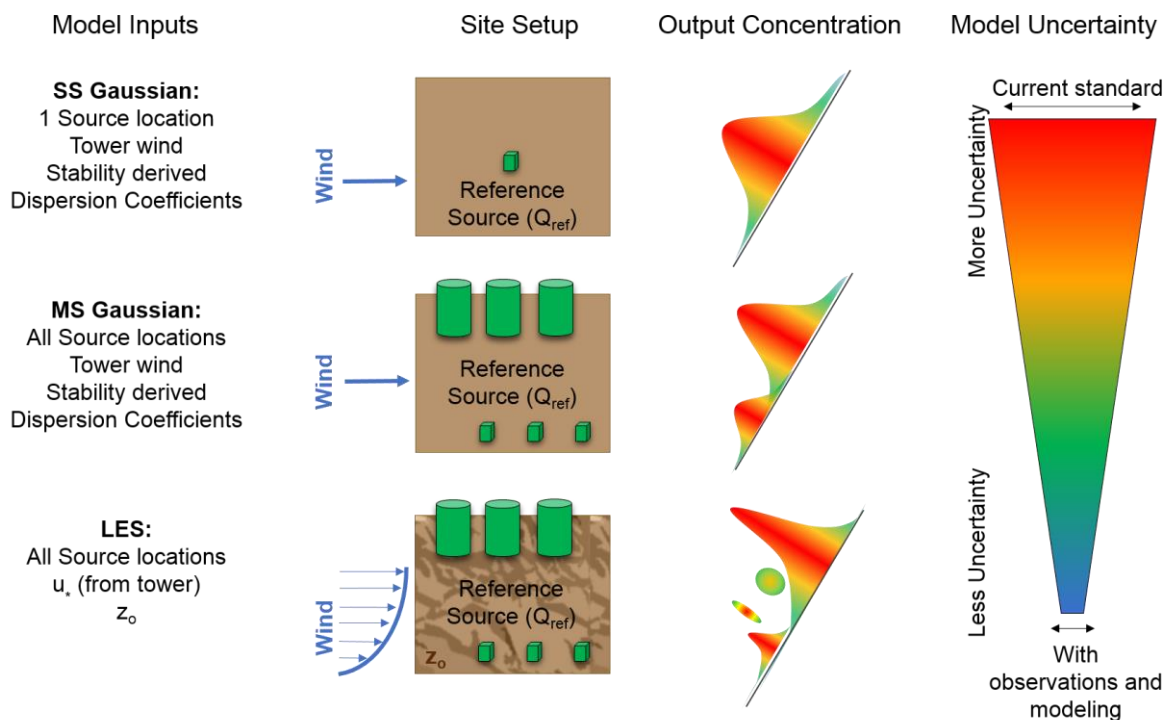


Figure 6. Finalized sampling strategy employed in this study showing actual measurements with increasing complexity and decreasing sample size.

5



## Source Determination Design



**Figure 7. Finalized source strength determination strategy employed in this study showing models with increasing complexity and decreasing uncertainty. In this schematic  $u_*$  is friction velocity and  $z_o$  is terrain roughness length.**

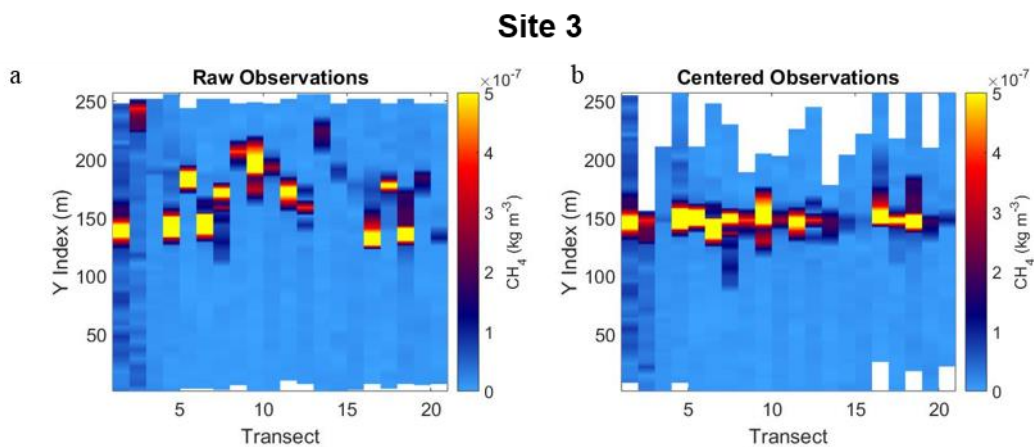


**Figure 8.** (a) Site 3 raw observations as indexed to the LES domain and (b) after they have been aligned with the peak of the LES plume.

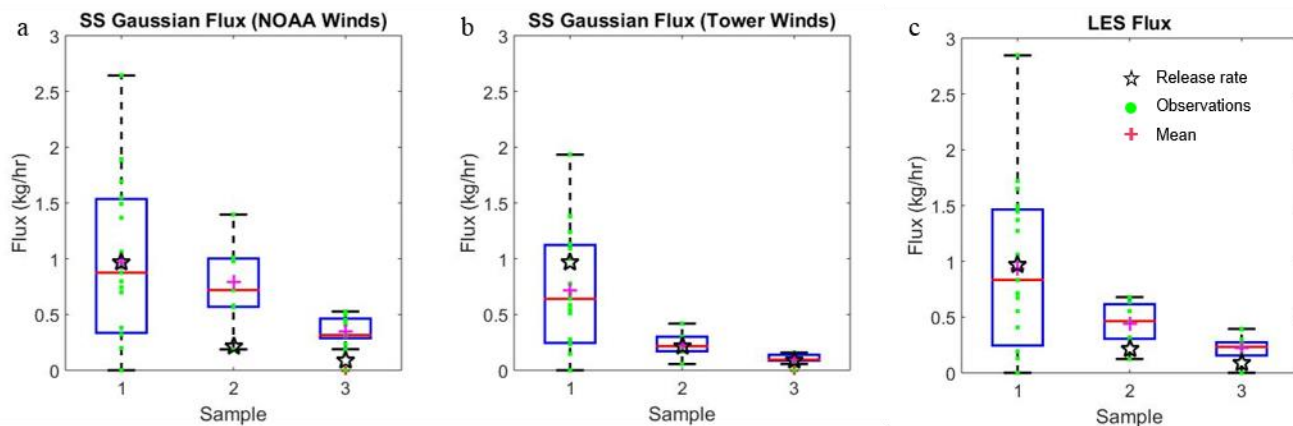


**Figure 9.** Results from three controlled release experiments for (a) the Gaussian approach using NOAA winds, (b) the Gaussian approach using tower measured winds and (c) from the LES. Box and whiskers plots show the 50% percentile (red), 25 and 75% percentile (blue) and minimum and maximum values (black). The mean is shown in magenta, green dots represent individual measurements and the black star is the actual release rate.

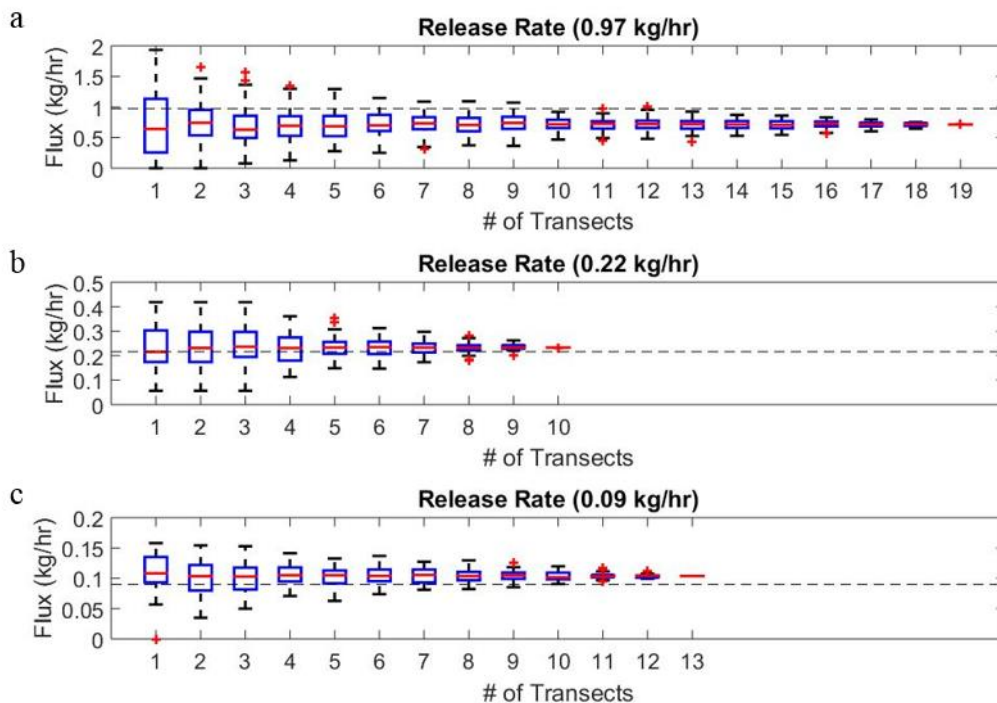
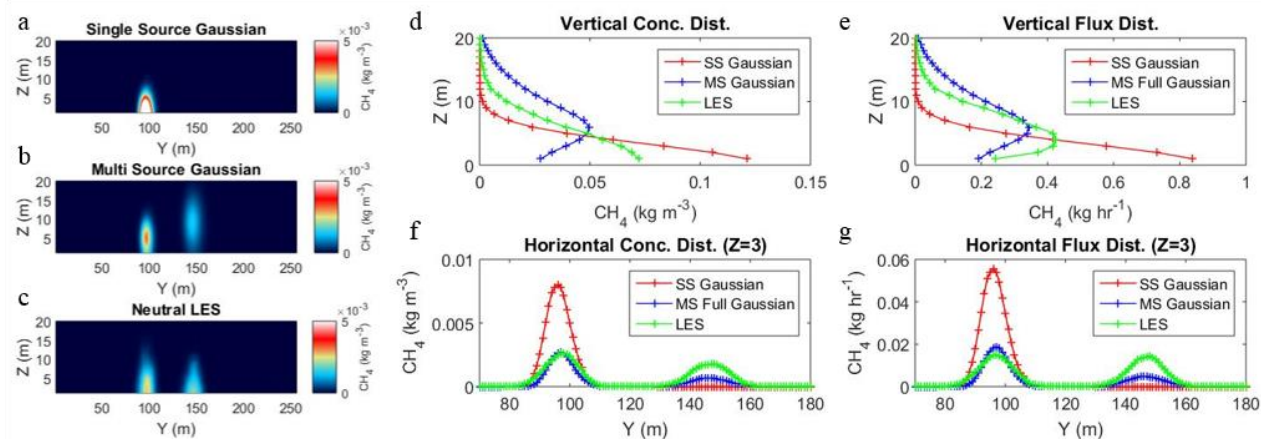


Figure 10. A comparison of the convergence of the plume rate by averaging randomly selected transects for (a) the 0.97 kg hr<sup>-1</sup> release rate, (b) the 0.22 kg hr<sup>-1</sup> release rate and (c) the 0.09 kg hr<sup>-1</sup> release rate. The actual release rate is shown as a dashed black line. Box and whiskers plots show the 50% percentile (red), 25 and 75% percentile (blue) and minimum and maximum values (black). Outliers are shown in red.



### Site 3



**Figure 11.** Comparison of three scenarios for Site 3 showing images of (a) single source Gaussian, (b) multi-source Gaussian and (c) averaged LES. The comparison of vertical distributions of (d) concentrations and (e) fluxes and of the horizontal distributions of (f) concentrations and (g) fluxes are also shown.

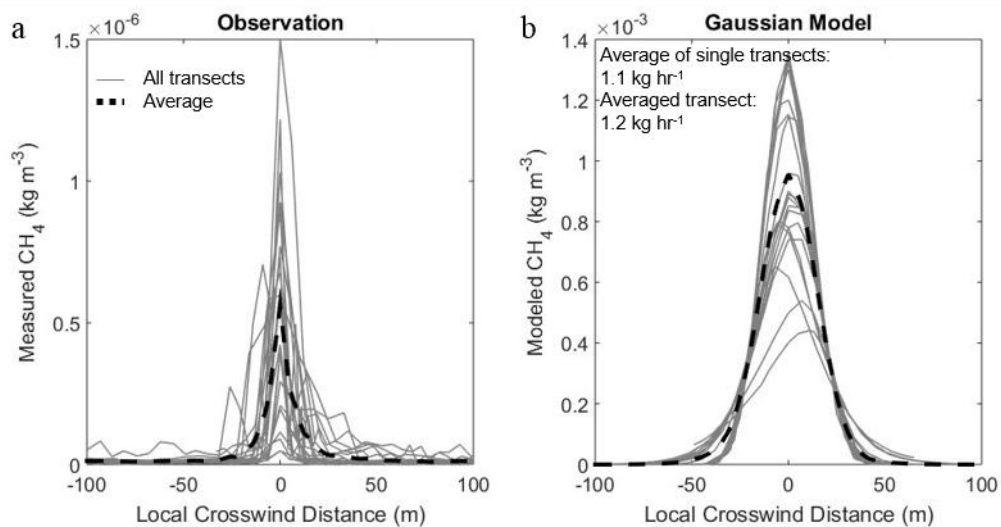


**Figure 12. (a) Observations of  $\text{CH}_4$  at Site 3 showing multiple downwind transects in gray and the averaged transect in black. (b) Gaussian outputs in gray along the same downwind transects and the averaged profile in black.**

5

10